Progress In Electromagnetics Research C, Vol. 110, 1–14, 2021

Applicability Analysis of the Phase Scanning in Antenna Arrays of Chirp Pulse Radars

Volodymyr G. Galushko* and Dmytro M. Vavriv

Abstract—In this paper, the space-and-time structure of the output signal of the antenna array (AA) of a chirp pulse radar is investigated in dependence on the frequency sweep range of the probe signal. Expressions are derived for calculating the output signals of the AA of a chirp pulse radar after optimal filtering in the case of beamforming using phase shifters and/or time-delay lines. Distortions of the space-time power pattern pertaining to the phase scanning method are analyzed in dependence on the frequency chirp range and scan angle. It is shown that these distortions are similar to the effects observed in the case of using taper windows for sidelobe suppression in the time and space (angular) domains. Based on the results obtained an applicability condition is suggested for the phase scanning in AAs of chirp pulse radars. It is shown that minor violations of this condition result in decreasing the amplitude and broadening of the main lobe and sidelobes in the AA space-time power pattern. In the case of strong violations of the applicability condition for the phase scanning the sidelobes of the angular directional pattern degrade, merging with the main one into a single quite broad maximum. The considered effects lead to deterioration of the range and azimuth resolution capabilities of radars and should be taken into account when selecting the taper window parameters.

1. INTRODUCTION

For approximately two decades before and during World War II, much activity in radar investigations, both theoretical and experimental, was focused on the use of antenna arrays (AAs) [1]. The result was the FuMG 41/42 "Mammut" radar built in Germany in 1944 on the basis of an electronically steerable phased antenna array (PAA), which is supposed to be the world's first system of the kind [2]. However, PAAs have not become widespread at that time since with transition to higher sounding frequencies, after invention of the resonant-cavity magnetron [3], preference was given to simpler antenna systems with mechanical beam scanning like, for example, parabolic antennas [4, 5].

The interest in AAs for radar applications was renewed in the early 1960s owing to the rapid advance in the digital signal processing and is still not calming down [6]. The progress in this field has also been strongly supported by essential breakthrough in microwave component industry and development of target processing algorithms. The availability of efficient transmit-receive modules [7] and target classification and recognition algorithms [8] has resulted in the appearance of multifunctional radars for ground and airborne applications [9]. According to the report of BCC (Business Communications Company) analysts [10] among the 5 key tendencies in radar technology for 2018 to 2022 there is ever increasing demand in active electronically scanned arrays. Antenna systems of the kind permit parameters of the signals (amplitude, frequency and phase) radiated and/or received by each element of the aperture to be controlled individually, thus providing the possibility to steer the AA beam electronically and adapt its shape to perform specific radar functions in rapidly changing conditions.

Received 11 December 2020, Accepted 2 February 2021, Scheduled 11 February 2021
* Corresponding author: Volodymyr G. Galushko (galushko@rian.kharkov.ua).
The authors are with the Institute of Radio Astronomy, National Academy of Sciences of Ukraine 4, Mystetstv St., Kharkiv 61002, Ukraine.

An essential advantage of the electronically scanned AA is the time required to switch the beam from one position to another which takes a few microseconds. This makes it possible to almost simultaneously track a great number of targets and make a quick survey of the specified scene, as well as to perform several radar functions in parallel, for example, target detection and tracking (multifunction radars). In addition, disuse of precision rotary devices allows essentially improving the design reliability and strength, with decreasing the weight and preserving the beam positioning accuracy. Another advantage of AAs is the possibility of exciting by a few coherent solid-state transmitters, thus increasing the radar performance figure and hence the detection range.

Strictly speaking, the AA beam should be steered through changing the time delay between the signals transmitted/received by elementary antennas. In the 2D case of a linear equidistant AA the incremental time delay $\Delta\tau_0$ between adjacent elements of the aperture is [6]

$$\Delta\tau_0 = \frac{l}{c}\sin\alpha_0, \tag{1}$$

where l is the AA spacing (separation between adjacent elements); c stands for the velocity of light in free space; and α_0 specifies the beam direction counted clockwise from the normal to the array. To form the appropriate time delays $\Delta\tau_0$, electronically controlled delay lines are necessary, which are rather complex, cumbersome and expensive to be connected to each elementary antenna of the AA [6]. For this reason, the phase scanning is more frequently used in practice, in which case phase shifters are applied instead of delay lines to introduce the required incremental phase shift $\Delta\varphi_0$ between adjacent elements of the AA,

$$\Delta\varphi_0 = \frac{2\pi l}{\lambda}\sin\alpha_0. \tag{2}$$

Comparison of Eqs. (1) and (2) shows that in the case of sufficiently narrow band signals the phase and time-delay scanning are practically identical, since $\Delta\tau_0$ is expressed through $\Delta\varphi_0$ as

$$\Delta\tau_0 = \frac{\Delta\varphi_0}{\omega_0}, \tag{3}$$

where $\omega_0 = 2\pi f_0$, with f_0 being the central (carrier) frequency of the signal.

As seen from Eq. (3), if $\Delta\varphi_0$ is frequency-invariant, the dime delay $\Delta\tau_0$ proves to be dependent on the signal carrier frequency f_0. This effect, which some authors (see, for example, [11, 12]) refer to as the "aperture effect", is exploited in frequency beam-scanning PAAs [13]. Thus, the time delay $\Delta\tau_0$ will not be the same for different spectral components of broadband signals that may affect the PAA directional pattern.

In the case of simple signals, for example, unmodulated rectangular pulses, the phase scanning can be expected to be applicable if all elementary antennas of a PAA are excited simultaneously, i.e., if the following condition holds

$$c\tau_p \geq L|\sin\alpha_0|, \tag{4}$$

where τ_p is the signal duration and L the array length.

Given that the signal spectrum width Δf relates to τ_p as $\Delta f \approx 1/\tau_p$, Equation (4) yields the following estimate of the PAA relative bandwidth

$$\frac{\Delta f}{f_0} = \frac{\lambda}{L|\sin\alpha_0|},$$

which quite agrees with the formulas for $\Delta f/f_0$ from [2, 14]. For example, in [14] $\Delta f/f_0$ is determined as (we slightly modified the original formula replacing $L\sin\alpha_0$ with $L|\sin\alpha_0|$ to secure $\Delta f > 0$)

$$\frac{\Delta f}{f_0} = 0.866 B_b \frac{\lambda}{L|\sin\alpha_0|}, \tag{5}$$

where B_b is the beam broadening factor associated with a nonuniform field distribution across the PAA aperture (for uniformly excited array $B_b = 1$). The bandwidth Δf in Eq. (5) is determined as the difference between the frequencies at which the PAA power gain is reduced to 3 dB level with respect to

its value at the central frequency f_0. Note that Eq. (5) allows estimating the PAA absolute bandwidth as

$$\Delta f = 0.866 B_b \frac{\lambda f_0}{L|\sin\alpha_0|} = 0.866 B_b \frac{c}{L|\sin\alpha_0|}, \tag{6}$$

which implies that Δf is inversely proportional to the "longitudinal" dimension of the array $L_{\|} = L|\sin\alpha_0|$, i.e., to its projection on the main beam direction.

Thus, the estimates in Eqs. (5) and (6) consider only frequency dependences of the PAA directivity characteristics. At the same time, amplitudes of different frequency components of the signal can essentially differ from one another. For this reason, analysis of possible distortions of the radar echo after optimal processing, associated with application of the phase scanning, requires considering not only spatial (angular) dependence of the PAA output signal but also its time structure.

The present study is aimed at investigating the space-time structure of the output signal of the PAA chirp pulse radar in dependence on the frequency sweep range of the sounding signal and analyzing the applicability condition for the phase scanning in such systems. As will be discussed in the next sections, the maximum achievable angular and range resolutions in radar systems with PAA are interrelated. For example, an attempt to improve the range resolution by increasing the frequency sweep range is limited by a finite length of the AA, which determines the angular resolution. We give a detailed explanation of this effect and propose approaches to find a trade-off between the angular and range resolutions. The obtained results are applicable to a wide range of PAA radar systems.

2. PROBLEM FORMULATION. GENERAL EXPRESSION FOR THE OUTPUT SIGNAL OF THE LINEAR EQUIDISTANT AA OF A CHIRP PULSE RADAR

Consider a linear equidistant AA consisting of N elementary antennas arranged symmetrically along the x-axis (see Fig. 1). The spacing between adjacent antennas is equal to l, such that the AA length L is $L = l(N-1)$.

A fixed point target T is located at a certain range R_T from the AA center coinciding with the origin of the Cartesian coordinates x, y. The target azimuth counted from the y-axis is equal to α_T.

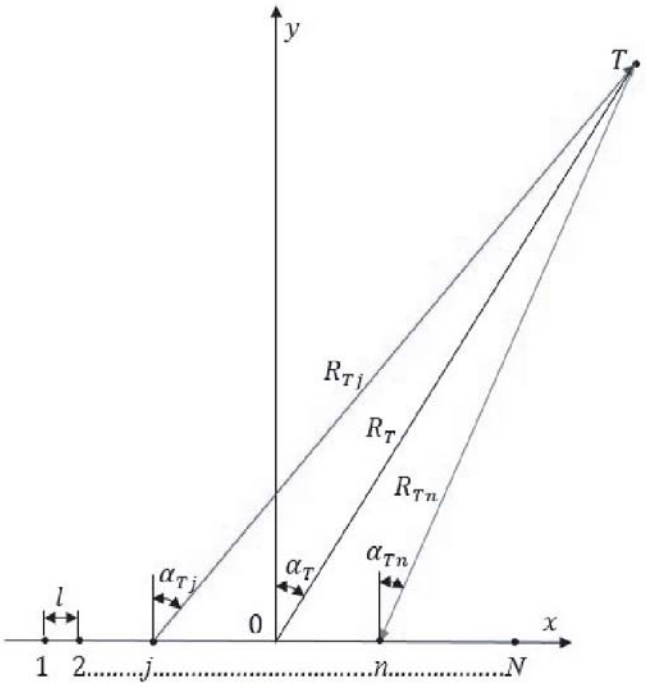

Figure 1. Problem geometry.

The AA radiating elements are all identical and transmit a chirp pulse waveform

$$u(t) = A_0(t)e^{-i\left[\omega_0(t-\tau_p/2)+\mu(t-\tau_p/2)^2/2+\varphi_0\right]}.$$

Here $A_0(t) = \begin{cases} A_0, & t \in [0,\tau_p], \\ 0, & t \notin [0,\tau_p], \end{cases}$ with A_0 and τ_p being the pulse amplitude and duration, respectively; $\omega_0 = 2\pi f_0$ is the carrier frequency; $\mu = 2\pi\Delta f/\tau_p$ is the slope of the phase modulation, with Δf being the frequency sweep width; and φ_0 is the initial phase.

The signal $u_j(t)$ from antenna j at the target position can be represented as

$$u_j(t) = G\left(\alpha_{Tj}, R_{Tj}\right) A_{0j}(t)e^{-i\left[\omega_0\left(t-\tau_{dj}-\tau_p/2\right)+\mu\left(t-\tau_{dj}-\tau_p/2\right)^2/2+\varphi_{0j}\right]}. \tag{7}$$

Here $G(\alpha_{Tj}, R_{Tj})$ is a factor allowing for the directional pattern of antenna j (α_{Tj} is the target azimuth with respect to antenna j) and attenuation of the signal on its path R_{Tj} from antenna j to the target; τ_{dj} is the total delay of the signal equal to the sum of the delay τ_{dAj} in antenna j with respect to a zero time moment $t = 0$ and the propagation delay τ_{dpj}; $A_{0j}(t) = \begin{cases} A_0, & t \in [\tau_{dj}, \tau_{dj}+\tau_p], \\ 0, & t \notin [\tau_{dj}, \tau_{dj}+\tau_p]; \end{cases}$ and φ_{0j} is the phase shift in antenna j.

The signal in Eq. (7) is reflected from the target and then is received by each antenna of the array. Thus, for the signal received by antenna n we can write

$$u_{nj}(t) = G\left(\alpha_{Tn}, R_{Tn}\right) G\left(\alpha_{Tj}, R_{Tj}\right) A_{0nj}(t)e^{-i\left[\omega_0\left(t-\tau_{dnj}-\tau_p/2\right)+\mu\left(t-\tau_{dnj}-\tau_p/2\right)^2/2+\varphi_{0nj}\right]}.$$

Here $G(\alpha_{Tn}, R_{Tn})$ is a factor allowing for the directional pattern of antenna n (α_{Tn} is the target azimuth as seen by antenna n) and attenuation of the target echo on its path R_{Tn} from the target to antenna n; τ_{dnj} is the total delay of the signal consisting of the delays in antennas j and n, $\tau_{dAnj} = \tau_{dAj} + \tau_{dAn}$, and propagation delay from antenna j to the target and then back to antenna n, $\tau_{dpnj} = \tau_{dpj} + \tau_{dpn}$; $A_{0nj}(t) = \begin{cases} \gamma A_0, & t \in [\tau_{dnj}, \tau_{dnj}+\tau_p], \\ 0, & t \notin [\tau_{dnj}, \tau_{dnj}+\tau_p], \end{cases}$ with γ being the target reflection factor; and φ_{0nj} is the total phase delay in antennas j and n.

The AA output $u_A(t)$ represents a sum of the signals received by each elementary antenna

$$u_A(t) = \sum_{j,n=1}^{N} u_{nj}(t). \tag{8}$$

For further analysis the distributions of the phase shifts φ_{0j} and time delays τ_{dAj} across the AA are assumed to be linear functions, *viz.*

$$\varphi_{0j} = -\Delta\varphi_0(j-1) \quad \text{and} \quad \tau_{dAj} = \Delta\tau_0(j-1),$$

where $\Delta\varphi_0$ and $\Delta\tau_0$ are, respectively, phase and time delay differences between elementary antennas $j+1$ and j of the AA (see Equations (1) and (2)).

Suppose that the AA length L is much shorter than the target range R_T, $L/R_T \ll 1$, and directional patterns of the elementary antennas are sufficiently broad such that

$$G(\alpha_{Tj}, R_{Tj}) \approx G(\alpha_T, R_T).$$

Then Eq. (8) can be written as

$$u_A(t) \approx G^2\left(\alpha_T, R_T\right) \sum_{j,n=1}^{N} A_{0nj}(t)e^{-i\left[\omega_0\left(t-\tau_{dnj}-\tau_p/2\right)+\mu\left(t-\tau_{dnj}-\tau_p/2\right)^2/2+\varphi_{0nj}\right]}, \tag{9}$$

where $\varphi_{0nj} = -\Delta\varphi_0(j+n-2)$ and $\tau_{dnj} \approx \frac{1}{c}[2R_T + L\sin\alpha_T - (j+n-2)l\sin\alpha_T] + \Delta\tau_0(j+n-2)$.

Noticing that summands with coincident sums $j+n$ in Eq. (9) are equal, we can go over to summation over a single index $m = j+n-1$. To that end, let us first sum terms for each $m = 1, 2, \ldots, 2N-1$. The result is $u_{Am}(t) \approx A_0\gamma G^2(\alpha_T, R_T)A_m(t)me^{-i[\omega_0(t-\tau_{dm}-\tau_p/2)+\mu(t-\tau_{dm}-\tau_p/2)^2/2+\varphi_{0m}]}$ for $m \in [1, N]$ and $u_{Am}(t) \approx A_0\gamma G^2(\alpha_T, R_T)A_m(t)(2N-m)e^{-i[\omega_0(t-\tau_{dm}-\tau_p/2)+\mu(t-\tau_{dm}-\tau_p/2)^2/2+\varphi_{0m}]}$ for $m \in [N+1, 2N-1]$, where $\varphi_{0m} = -\Delta\varphi_0(m-1)$, $\tau_{dm} \approx \frac{1}{c}[2R_T + L\sin\alpha_T - (m-1)l\sin\alpha_T] + \Delta\tau_0(m-1)$,

and $A_m(t) = \begin{cases} 1, & t \in [\tau_{dm}, \tau_{dm} + \tau_p], \\ 0, & t \notin [\tau_{dm}, \tau_{dm} + \tau_p]. \end{cases}$ Finally, combining these two expressions and making summation over m, we obtain

$$u_A(t) \approx A_0 \gamma G^2(\alpha_T, R_T) \sum_{m=1}^{2N-1} A_m(t) (N - |N - m|) e^{-i\left[\omega_0(t-\tau_{dm}-\tau_p/2)+\mu(t-\tau_{dm}-\tau_p/2)^2/2+\varphi_{0m}\right]}. \quad (10)$$

Thus, we have expressed the output signal of a linear equidistant AA as a function of the array parameters, time, and target position. This signal undergoes optimal filtering whose procedure is considered in the next Section.

3. OPTIMAL PROCESSING OF THE AA OUTPUT SIGNAL. SPACE-TIME PATTERN OF THE AA

As known (see, for example, [15]), the optimal algorithm of chirp pulse compression consists in convolution of the received signal with the reference (transmitted) signal $u_r(t)$. Let us select in the capacity of $u_r(t)$ the chirp pulse of unit amplitude associated with transmission of antenna N, *viz.*

$$u_r(t) = A_r(t) e^{-i\left[\omega_0(t-\tau_{dr}-\tau_p/2)+\mu(t-\tau_{dr}-\tau_p/2)^2/2+\varphi_{0r}\right]}, \quad (11)$$

where $\tau_{dr} = \Delta\tau_0(N-1)$, $\varphi_{0r} = -\Delta\varphi_0(N-1)$ and $A_r(t) = \begin{cases} 1, & t \in [\tau_{dr}, \tau_{dr} + \tau_p], \\ 0, & t \notin [\tau_{dr}, \tau_{dr} + \tau_p]. \end{cases}$.

In practice, it is more convenient to calculate the convolution integral in the spectral domain based on the convolution theorem [16]. Then, with account of Eq. (10), the output signal of the compression filter $u_c(t)$ can be represented as

$$u_c(t) = \int_{-\infty}^{\infty} S_r^*(\omega) S_A(\omega) e^{-i\omega t} d\omega = A_0 \gamma G^2(\alpha_T, R_T) \sum_{m=1}^{2N-1} (N - |N - m|) \int_{-\infty}^{\infty} S_r^*(\omega) S_{Am}(\omega) e^{-i\omega t} d\omega. \quad (12)$$

Here

$$S_r(\omega) = \frac{1}{2\pi} \int_{\tau_{dr}}^{\tau_{dr}+\tau_p} u_r(t) e^{i\omega t} dt \quad (13)$$

is the reference signal spectrum (asterisk "*" means the complex conjugation) and

$$S_{Am}(\omega) = \frac{1}{2\pi} \int_{\tau_{dm}}^{\tau_{dm}+\tau_p} u_{Am}(t) e^{i\omega t} dt, \quad (14)$$

where

$$u_{Am}(t) = A_m(t) e^{-i\left[\omega_0(t-\tau_{dm}-\tau_p/2)+\mu(t-\tau_{dm}-\tau_p/2)^2/2+\varphi_{0m}\right]}.$$

Thus, to find $u_c(t)$, it is necessary to calculate the integral

$$u_{cm}(t) = \int_{-\infty}^{\infty} S_r^*(\omega) S_{Am}(\omega) e^{-i\omega t} d\omega. \quad (15)$$

Substitution of Eqs. (13) and (14) into Eq. (15) with account of the Dirac delta function definition, $\delta(x) = \frac{1}{2\pi} \int_{-\infty}^{\infty} e^{i\omega x} d\omega$ [17], yields

$$u_{cm}(t) = \frac{1}{2\pi} e^{-i\Delta\varphi_0(N-m)} \int_{-\tau_p/2}^{\tau_p/2} \int_{-\tau_p/2}^{\tau_p/2} e^{i\omega_0(t'-t'')} e^{i\mu(t'-t'')(t'+t'')/2} \delta\left(t + t' - t'' + \tau_{dr} - \tau_{dm}\right) dt' dt''.$$

Changing the integration variables to the sum $\xi = t' + t''$ and difference $\rho = t' - t''$ ones, $u_{cm}(t)$ can be represented as

$$u_{cm}(t) = \frac{1}{4\pi} e^{-i\Delta\varphi_0(N-m)} \left\{ \int\limits_{-\tau_p}^{0} d\rho \int\limits_{-\rho-\tau_p}^{\rho+\tau_p} d\xi + \int\limits_{0}^{\tau_p} d\rho \int\limits_{\rho-\tau_p}^{-\rho+\tau_p} d\xi \right\} e^{i(\omega_0\rho+\mu\rho\xi/2)} \delta(t+\rho+\tau_{dr}-\tau_m).$$

The integrals over ξ are easily calculated, and with account of the expressions for τ_{dr} and τ_m (see explanations to Equations (11) and (12)), we obtain

$$\begin{aligned} u_{cm}\left(\tilde{t}\right) &= \frac{1}{\pi\mu} e^{-i\Delta\varphi_0(N-m)} \left\{ \int\limits_{-\tau_p}^{0} e^{i\omega_0\rho} \frac{\sin\left[\mu\rho\left(\tau_p+\rho\right)/2\right]}{\rho} \delta\left[\tilde{t}+\rho-(N-m)\Delta\right] d\rho \right. \\ &\left. + \int\limits_{0}^{\tau_p} e^{i\omega_0\rho} \frac{\sin\left[\mu\rho(\tau_p-\rho)/2\right]}{\rho} \delta\left[\tilde{t}+\rho-(N-m)\Delta\right] d\rho \right\}, \end{aligned} \tag{16}$$

where $\tilde{t} = t - 2R_T/c$ and $\Delta = \frac{l}{c}\sin\alpha_T - \Delta\tau_0$. As can be seen, the first term in Eq. (16) contributes to $u_{cm}(\tilde{t})$ provided that $(N-m)\Delta \le \tilde{t} \le (N-m)\Delta + \tau_p$, while the second one if $(N-m)\Delta \ge \tilde{t} \ge (N-m)\Delta - \tau_p$. Then, making use of the sifting property of the Dirac delta function, we finally arrive at

$$\underset{\left|\tilde{t}-(N-m)\Delta\right|\le\tau_p}{u_{cm}\left(\tilde{t}\right)} = \frac{1}{\pi\mu} e^{-i\{\omega_0\left[\tilde{t}-\Delta(N-m)\right]+\Delta\varphi_0(N-m)\}} \frac{\sin\left\{\mu\left[\tilde{t}-\Delta(N-m)\right]\left(\tau_p-\left|\tilde{t}-\Delta(N-m)\right|\right)/2\right\}}{\tilde{t}-\Delta(N-m)}. \tag{17}$$

So, now we are in position to calculate the pulse compression filter output $u_c(\tilde{t})$ through substitution of Eq. (17) into Eq. (12) with account of Eq. (16) and summation of the result over m. Since with fixed parameters of the AA and angle α_0 the response of the pulse compression filter $u_c(\tilde{t})$ depends not only on the time alone but also on the target angular position, in what follows we will refer to it as the AA space-time pattern and denote as $u_c(\tilde{t}, \alpha_T)$. In the next Section, $u_c(\tilde{t}, \alpha_T)$ is analyzed as a function of the AA parameters and characteristics of the sounding signal.

4. APPLICABILITY CONDITION OF THE PHASE SCANNING. ANALYSIS OF NUMERICAL RESULTS

As follows from Eq. (17), in the case of the time-delay scanning (i.e., through changing $\Delta\tau_0 = \frac{l}{c}\sin\alpha_0$ only, with $\Delta\varphi_0 = 0$), the partial signals $u_{cm}(\tilde{t})$ in Eq. (12) will be summed with no loss if $\alpha_0 = \alpha_T$, i.e., when the array antenna is precisely aimed at the target. In this case $\Delta = 0$ and Equation (12) yields

$$\underset{|\tilde{t}|\le\tau_p}{u_c^{(td)}(\tilde{t}, \alpha_T)} = \frac{A_0\gamma}{\pi\mu} N^2 G^2(\alpha_T) e^{-i\omega_0\tilde{t}} \frac{\sin\left[\mu\tilde{t}\left(\tau_p-|\tilde{t}|\right)/2\right]}{\tilde{t}}.$$

(Here and below, we ignore the range dependence of the factor $G(\alpha_T, R_T)$ assuming that it changes but slightly over the characteristic scale of the function $\sin[\mu\tilde{t}(\tau_p-|\tilde{t}|)/2]/\tilde{t}$). As expected, the output signal of the pulse compression filter in the case under consideration is N^2 times stronger than that received by a single elementary antenna.

In the case of phase scanning (i.e., through changing $\Delta\varphi_0 = \frac{2\pi l}{\lambda}\sin\alpha_0$ with $\Delta\tau_0 = 0$) summation in Eq. (12) will be performed with some loss even if the AA is precisely aimed at the target ($\alpha_0 = \alpha_T$), since Equation (17) implies that

$$\underset{\left|\tilde{t}-(N-m)\Delta\right|\le\tau_p}{u_{cm}\left(\tilde{t}\right)} = \frac{1}{\pi\mu} e^{-i\omega_0\tilde{t}} \frac{\sin\left\{\frac{\mu}{2}\left[\tilde{t}-\frac{l}{c}(N-m)\sin\alpha_T\right]\left(\tau_p-\left|\tilde{t}-\frac{l}{c}(N-m)\sin\alpha_T\right|\right)\right\}}{\tilde{t}-\frac{l}{c}(N-m)\sin\alpha_T}.$$

Therefore, the output signal $u_c^{(ph)}(\tilde{t},\alpha_T)$ will comprise partial signals $\underset{|\tilde{t}-(N-m)\Delta|\le\tau_p}{u_{cm}(\tilde{t})}$ shifted relative to one another along the time axis $\tilde{t}$ by $\Delta_{sm}=\frac{l}{c}(N-m)\sin\alpha_T$, and certain portion of target echo power will be lost. The exception is the case $\alpha_T=0$ where the time shift between adjacent components of the signal $u_c^{(ph)}(\tilde{t},\alpha_T)$ is equal to 0.

The amount of the loss in the target echo power can be regarded as negligibly small if the maximum shift $\Delta_{s\max}=\frac{l}{c}(N-1)|\sin\alpha_T|=\frac{L}{c}|\sin\alpha_T|$ of the partial components of the signal $u_c^{(ph)}(\tilde{t},\alpha_T)$ is much less than their characteristic width $\Delta\tilde{t}$, i.e., if the following inequality holds

$$\frac{\Delta_{s1}}{\Delta\tilde{t}}\ll 1. \tag{18}$$

It is easy to show that the zero-level width of the functions $u_{cm}(\tilde{t})$ is

$$\Delta\tilde{t}=\tau_p\left[1-\sqrt{1-4/B}\right], \tag{19}$$

where $B=\Delta f\tau_p$ stands for the time-bandwidth product of the chirp pulse.

Then, the condition in Eq. (18) for $B\gg 1$ can be brought to the form

$$\frac{BL|\sin\alpha_T|}{2c\tau_p}\ll 1.$$

Taking into account that the value $\frac{c\tau_p}{2B}=\Delta R$ determines the range resolution, the applicability condition of the phase scanning in Eq. (18) can be represented as

$$\varsigma=\frac{L|\sin\alpha_T|}{4\Delta R}\ll 1. \tag{20}$$

Thus, the phase scanning is applicable in AAs of chirp pulse radars if the "longitudinal" dimension of the array $L_\parallel=L|\sin\alpha_0|$ is much smaller than four range bins. Note that inequality in Eq. (20) permits estimating the relative frequency sweep $\Delta f/f_0$ as

$$\frac{\Delta f}{f_0}\ll\frac{2\lambda}{L|\sin\alpha_T|},$$

which value quite agrees with the estimate in Eq. (5) for the PAA relative bandwidth [14]. Accordingly, for the absolute value of the frequency sweep Δf we have

$$\Delta f\ll\frac{2c}{L|\sin\alpha_T|}.$$

Shown in Fig. 2 as 3D relief plots are normalized space-time power patterns (STPP) of a linear equidistant AA calculated for the scan angles $\alpha_0=10^\circ$ (a), $\alpha_0=19^\circ$ (b), and $\alpha_0=60^\circ$ (c) in dependence on the time $\tilde{t}$ and target azimuth α_T for the cases of time-delay, $u_{\text{cnorm}}^{(td)}(\tilde{t},\alpha_T)=|u_c^{(td)}(\tilde{t},\alpha_T)|^2/|u_c^{(td)}(\tilde{t}=0,\ \alpha_T=\alpha_0)|^2$ (left panels) and phase, $u_{\text{cnorm}}^{(ph)}(\tilde{t},\alpha_T)=|u_c^{(ph)}(\tilde{t},\alpha_T)|^2/|u_c^{(td)}(\tilde{t}=0,\ \alpha_T=\alpha_0)|^2$ (right panels) scanning. The sounding signal represents a chirp pulse of length $\tau_p=0.1\,\mu$s with the frequency sweep $\Delta f=400\,$MHz and central frequency $f_0=10\,$GHz ($\lambda=3\,$cm). The array spacing equals a half wavelength $l=\lambda/2=1.5\,$cm, and the number of the elementary antennas is $N=133$ ($L=198\,$cm). The directional pattern of the elementary antenna is described as $\cos^2\alpha_0$. (Note that the same values of the AA parameters are used in all the calculations presented in this paper.) The factor ς for $\alpha_T=\alpha_0=10^\circ$, 19° and 60° assumes the values of approximately 0.23 ($\varsigma\ll 1$), 0.43 ($\varsigma<1$) and 1.14 ($\varsigma>1$). Note that according to Eq. (6), the bandwidth of the PAA under consideration for $\alpha_0=19^\circ$ is 403 MHz, i.e., is practically equal to the frequency sweep range $\Delta f=400\,$MHz used in the calculations, and $\alpha_0=60^\circ$ corresponds to the conventionally accepted value of the maximum scan angle [6].

As can be seen, the $u_{\text{cnorm}}^{(td)}(\tilde{t},\alpha_T)$ pattern preserves its structure in the course of changing the scan angle α_0. Only the familiar broadening of the main beam and sidelobes is observed over the angular coordinate α_T associated with decreasing the directivity due to reducing the effective ("transverse") length $L_\perp=L\cos\alpha_0$ of the AA as α_0 increases. At the same time, the $u_{\text{cnorm}}^{(ph)}(\tilde{t},\alpha_T)$ pattern is essentially

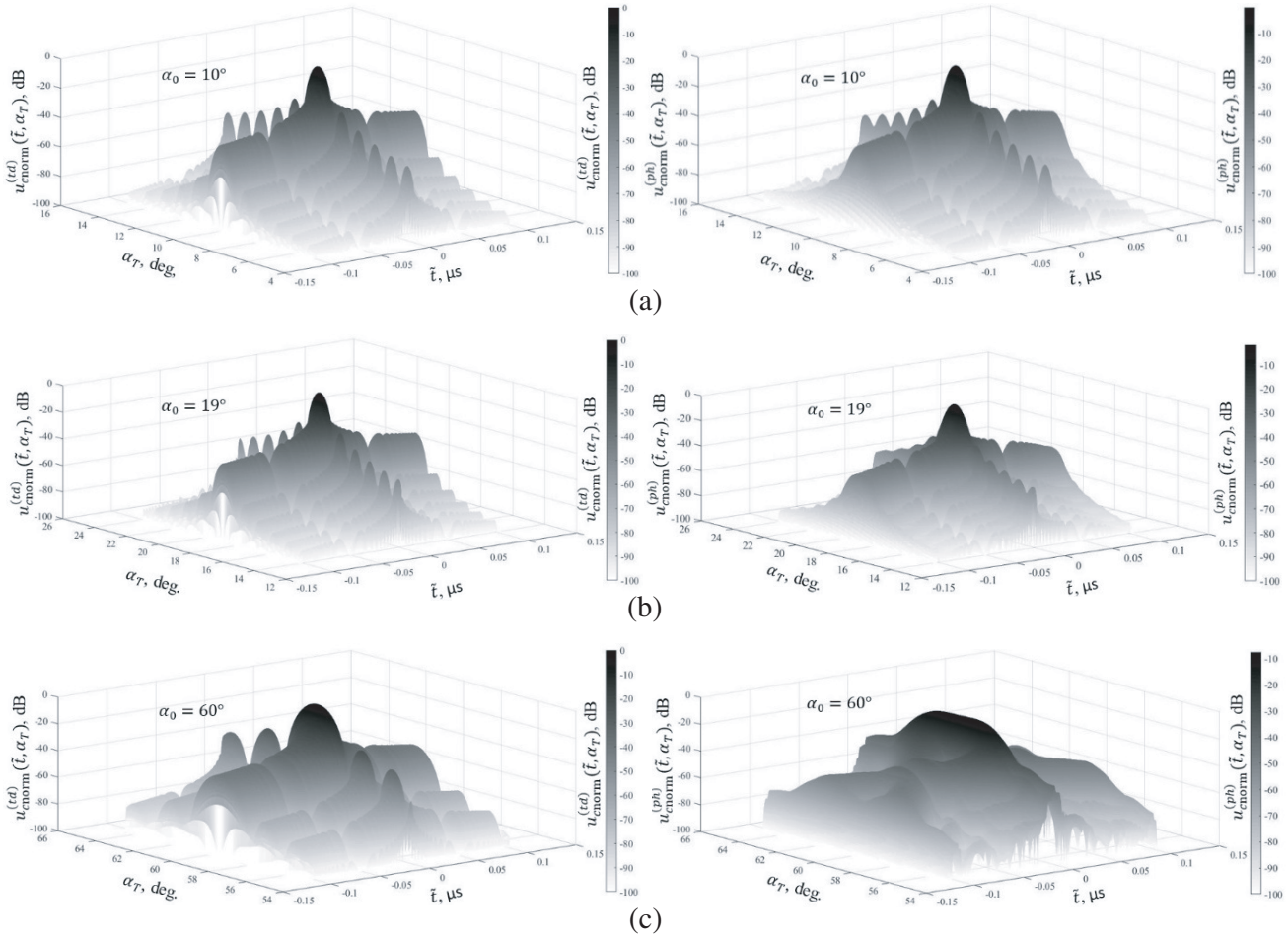

Figure 2. 3D plots of normalized STPPs of a linear equidistant AA calculated for the scan angles (a) $\alpha_0 = 10°$, (b) $\alpha_0 = 19°$ and (c) $\alpha_0 = 60°$ in dependence on the time $\tilde{t}$ and target azimuth α_T for the cases of time-delay (left panels) and phase (right panels) scanning.

dependent on the scan angle α_0. Thus, for $\alpha_0 = 10°$, when the condition in Eq. (20) is strictly met since $\varsigma = 0.23 \ll 1$, the $u^{(ph)}_{\text{cnorm}}(\tilde{t}, \alpha_T)$ and $u^{(td)}_{\text{cnorm}}(\tilde{t},\ \alpha_T)$ patterns are practically coincident (see Fig. 2(a)). One can see just a minor decrease in the main lobe amplitude (approximately by 0.5 dB) and a slight increase of the minima in the case of the phase scanning as compared with the time-delay one. With $\alpha_0 = 19°$, when the condition in Eq. (20) is slightly violated ($\varsigma = 0.43 < 1$), the difference between $u^{(ph)}_{\text{cnorm}}(\tilde{t}, \alpha_T)$ and $u^{(td)}_{\text{cnorm}}(\tilde{t}, \alpha_T)$ is more noticeable (see Fig. 2(b)) despite the fact that the bandwidth of the given PAA as estimated after Eq. (6) is about 403 MHz, and this value exceeds the sweep frequency range of the chirp pulse by just 3 MHz. In particular, the main maximum of $u^{(ph)}_{\text{cnorm}}(\tilde{t}, \alpha_T)$ is lower than that of $u^{(td)}_{\text{cnorm}}(\tilde{t}, \alpha_T)$ by approximately 1.72 dB and slightly wider along the angular coordinate than the latter. Also, the minima become yet less pronounced than the case $\alpha_0 = 10°$.

With a strong violation of the condition in Eq. (20), whose situation corresponds to $\alpha_0 = 60°(\varsigma = 1.14 > 1)$, the $u^{(ph)}_{\text{cnorm}}(\tilde{t}, \alpha_T)$ pattern becomes drastically distorted. This is clearly observed from the sections of $u^{(td)}_{\text{cnorm}}(\tilde{t}, \alpha_T)$ and $u^{(ph)}_{\text{cnorm}}(\tilde{t}, \alpha_T)$ shown in Fig. 2 by the planes $\alpha_T = \alpha_0$ and $\tilde{t} = 0\,\mu$s, which are presented in Fig. 3. As can be seen, increasing the angle α_0 in the case of the phase scanning results in decreasing the main maximum of the $u^{(ph)}_{\text{cnorm}}(\tilde{t},\ \alpha_T = \alpha_0)$ dependence and its broadening as compared with the main lobe of $u^{(td)}_{\text{cnorm}}(\tilde{t},\ \alpha_T = \alpha_0)$, and also in lowering the relative sidelobe level (SLL), $SLL^{(ph)}_{\tilde{t}}$

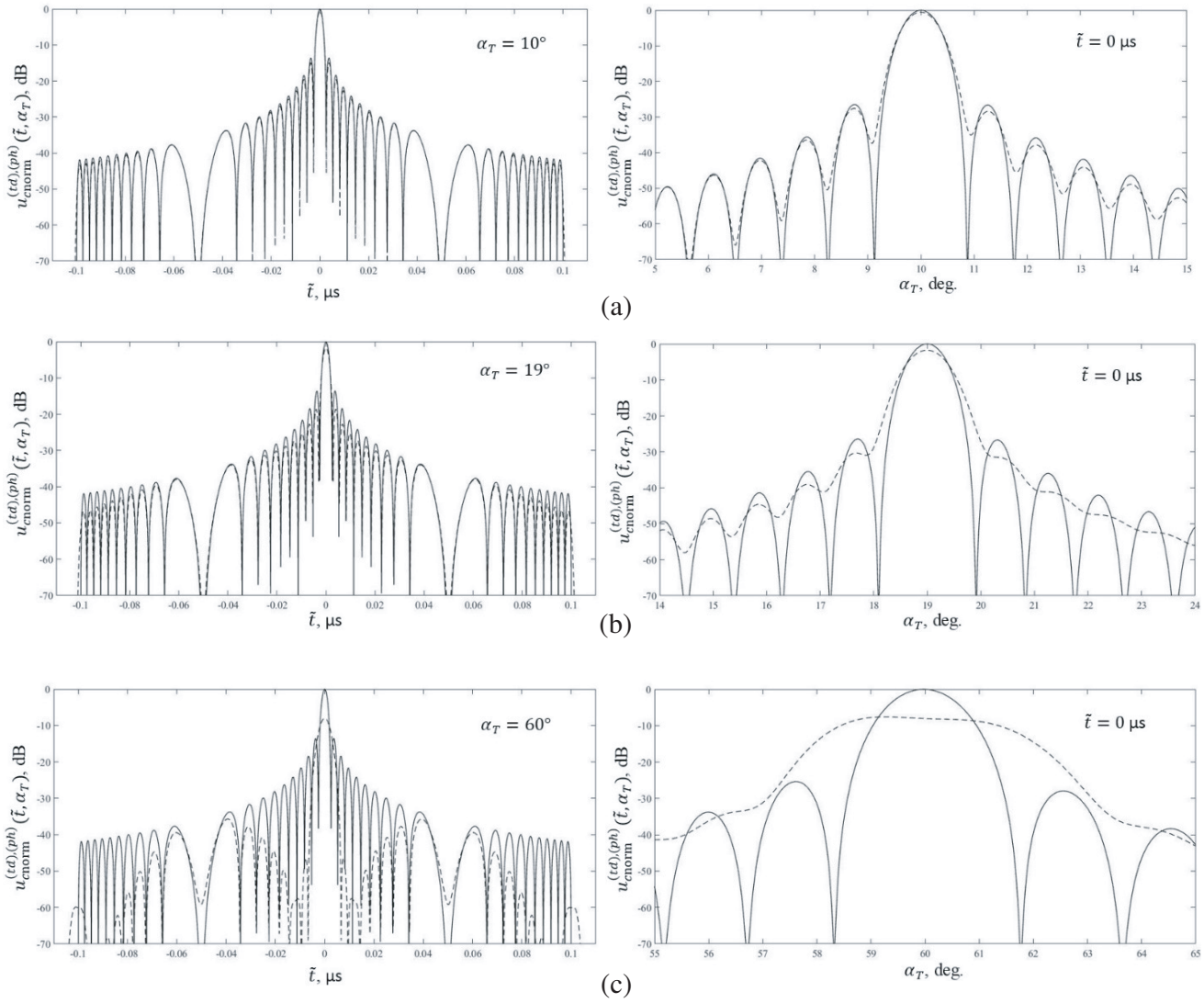

Figure 3. Sections of the $u^{(td)}_{\text{cnorm}}(\tilde{t}, \alpha_T)$ and $u^{(ph)}_{\text{cnorm}}(\tilde{t}, \alpha_T)$ patterns presented in Fig. 2 by the planes $\alpha_T = \alpha_0$ (left panels) and $\tilde{t} = 0\,\mu\text{s}$ (right panels) for the cases of the time-delay (solid lines) and phase (dashed lines) scanning.

(see the dashed lines in the left panels of Fig. 3).

In addition, the matched filter output of the chirp pulse compression radar $u^{(ph)}_{\text{cnorm}}(\tilde{t},\ \alpha_T = \alpha_0)$ stretches along the time axis $\tilde{t}$. Thus, for $\alpha_0 = 60°$ its length is about $\pm 0.1055\,\mu\text{s}$, whereas duration of $u^{(td)}_{\text{cnorm}}(\tilde{t},\ \alpha_T = \alpha_0)$ is equal to double length of the sounding pulse τ_p, i.e., to $\pm 0.1\,\mu\text{s}$. It is quite evident that this effect is because the time-delay differences between m-th components of the signal $u_c(\tilde{t})$ are not compensated in the case of the phase scanning. As a result, the length of the pulse compression filter is equal to $2(\tau_p + L_{\|}/c)$, as can be seen from Eq. (17).

As to decreasing and broadening the main maximum and reducing the relative SLL in the case of the phase scanning, these effects likely occur due to amplitude modulation of the effective pulses transmitted by the PAA toward a target and then received from it. Actually, transmission of chirp pulses with a fixed phase shifts $\Delta\varphi_0 = \frac{2\pi l}{\lambda}\sin\alpha_0$ between the elementary antennas can be treated in terms of frequency scanning antenna arrays [13]. Indeed, if the instantaneous frequency f_{ins} of a chirp pulse changes during its transmission within the range $f_{ins} = f_0 \pm \Delta f/2$, the main lobe position will vary

between the limits $\alpha_0 = \sin^{-1} \frac{c\Delta\varphi_0}{2\pi l(f_0 \pm \Delta f/2)}$. As a result, the pulse transmitted toward the target will be amplitude modulated by the PAA pattern. A similar modulation occurs in the course of reception of the target echo. Because of this, the signal waveform at the pulse compression filter input can essentially differ from the square one. So, this modulation can be regarded as a result of applying a kind of a taper window to the transmitted/received pulses, which is always accompanied by the effects similar to those described above (see, for example, [15, 18]).

It should be noted that high-level sidelobes in the matched filter output can mask weak target echoes against strong reflections from other targets and clutter or cause false detections. For this reason, various kinds of taper windows (Hamming, Blackman, etc.) are used in the time or frequency domain for sidelobe suppression. As a rule, these are standard windows developed for optimum estimation of the spectral amplitude of narrowband signals [19]. The choice of a particular window always faces an alternative between broadening and decreasing the main maximum, which affect the range resolution and signal-to-noise ratio, and reduce the SLL. Since similar effects can be observed in phased array radars, it might be necessary to take these into account when selecting the taper window parameters.

Analysis of the $u^{(td)}_{\text{cnorm}}(\tilde{t} = 0, \alpha_T)$ sections presented in the right panels of Fig. 3 shows that their structure is practically independent of the scan angle α_0, except for the familiar broadening of the main and minor lobes as α_0 increases. At the same time, the $u^{(ph)}_{\text{cnorm}}(\tilde{t} = 0, \alpha_T)$ distributions depend essentially on α_0. Thus, if $\alpha_0 = 10^\circ$ ($\varsigma = 0.23 \ll 1$), the $u^{(ph)}_{\text{cnorm}}(\tilde{t} = 0, \alpha_T)$ and $u^{(td)}_{\text{cnorm}}(\tilde{t} = 0, \alpha_T)$ dependences are practically identical (see Fig. 3(a)). One can see only a slight difference in the main and minor lobe levels, as well as in the width of the main maximum and depth of minima. With $\alpha_0 = 19^\circ$ ($\varsigma = 0.43 < 1$), in addition to the noticeable decrease of the main maximum discussed above when analyzing the $u^{(td)}_{\text{cnorm}}(\tilde{t}, \alpha_T = \alpha_0)$ and $u^{(ph)}_{\text{cnorm}}(\tilde{t}, \alpha_T = \alpha_0)$ dependences, a significant increase is observed in the main lobe width $\Delta\alpha^{(ph)}_{-20\,\text{dB}}$ at the $-20\,\text{dB}$ level, which is approximately half as much again as the respective width $\Delta\alpha^{(td)}_{-20\,\text{dB}}$ of $u^{(td)}_{\text{cnorm}}(\tilde{t} = 0, \alpha_T)$. The minima flatten out significantly and practically degrade. When $\alpha_0 = 60^\circ$ ($\varsigma = 1.14 > 1$) the sidelobes in $u^{(ph)}_{\text{cnorm}}(\tilde{t}, \alpha_T = \alpha_0)$ finally disappear, merging with the main lobe in a single broad maximum with $\Delta\alpha^{(ph)}_{-20\,\text{dB}} \approx 5.7^\circ$. This maximum is lower than the main lobe of the $u^{(td)}_{\text{cnorm}}(\tilde{t} = 0, \alpha_T)$ dependence by approximately 8 dB and is shifted with respect to the latter by nearly 0.72° toward smaller α_T. This effect seriously deteriorates the signal-to-noise ratio, angular resolution, and accuracy of estimating the target azimuth. Most likely, it arises due to uncompensated time-delay difference between m-th components of the signal $u_{(ph)}(\tilde{t})$. Indeed, Equation (17) implies that maxima and minima of component m of the signal $u_{(ph)}(\tilde{t})$ in the case of the phase scanning are shifted by the value $\Delta^{(ph)}_{\tilde{t}} = \frac{l}{c} \sin\alpha_T$ along the time axis $\tilde{t}$ relative to the respective maxima and minima of component $m + 1$. Thus, with changing α_T in a certain vicinity to α_0 the delay $\Delta^{(ph)}_{\tilde{t}}$ may prove sufficient for the sidelobes in the $u^{(ph)}_{\text{cnorm}}(\tilde{t} = 0, \alpha_T)$ dependence being partially or completely suppressed.

Figure 4 presents ratios of amplitudes $u^{(td)}_{\text{cnorm}}(0, \alpha_0)/u^{(ph)}_{\text{cnorm}}(0, \alpha_0)$ (solid line) and characteristic widths (at the $-20\,\text{dB}$ level) $\Delta\alpha^{(ph)}_{-20\,\text{dB}}/\Delta\alpha^{(td)}_{-20\,\text{dB}}$ (dashed line) and $\Delta\tilde{t}^{(ph)}_{-20\,\text{dB}}/\Delta\tilde{t}^{(td)}_{-20\,\text{dB}}$ (dash-and-dot line) of the output signals of the pulse compression filter in dependence on the frequency sweep range Δf of the chirp pulse. The results have been obtained for the pulse length $\tau_p = 0.1\,\mu\text{s}$, scan angle $\alpha_0 = 30^\circ$, and increment in Δf equal to 100 MHz. The values of the above ratios calculated at these discrete points (these are marked by symbols) have been approximated using the "spline" option in the Origin 8.1 program. With the given parameters of the AA and sounding pulse, the ratio ς in Eq. (20) changes linearly with Δf from 0.158 at $\Delta f = 100\,\text{MHz}$ to 1.108 at $\Delta f = 700\,\text{MHz}$. As can be seen, with increasing Δf the main maximum of the $u^{(ph)}_{\text{cnorm}}(\tilde{t}, \alpha_T)$ pattern monotonically decreases in magnitude and broadens over the time and angular coordinates with respect to that of the $u^{(td)}_{\text{cnorm}}(\tilde{t}, \alpha_T)$ pattern.

Note that the bandwidth of the PAA with the given parameters as estimated from Eq. (6) is equal to about 262.4 MHz. With this value of Δf the main maximum of the $u^{(ph)}_{\text{cnorm}}(\tilde{t}, \alpha_T)$ pattern is lower by approximately 1.85 dB than that of the $u^{(td)}_{\text{cnorm}}(\tilde{t}, \alpha_T)$ pattern and nearly 1.13 and 1.28 times wider

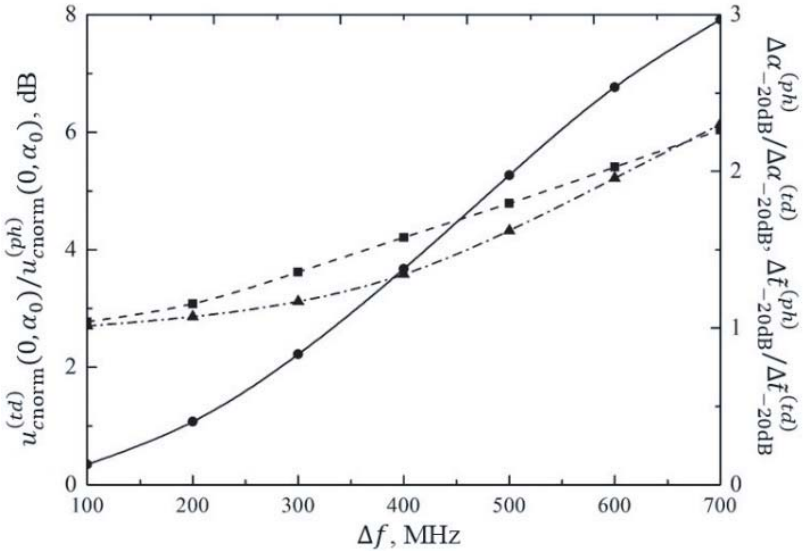

Figure 4. Ratios of the amplitudes $u^{(td)}_{\text{cnorm}}(0,\alpha_0)/u^{(ph)}_{\text{cnorm}}(0,\alpha_0)$ (solid line) and characteristic widths (at the -20 dB level) $\Delta\alpha^{(ph)}_{-20\,\text{dB}}/\Delta\alpha^{(td)}_{-20\,\text{dB}}$ (dashed line) and $\Delta\tilde{t}^{(ph)}_{-20\,\text{dB}}/\Delta\tilde{t}^{(td)}_{-20\,\text{dB}}$ (dash-and-dot line) of the main maxima of the pulse compression filter output in dependence on the frequency sweep range Δf calculated for a chirp pulse of length $\tau_p = 0.1\,\mu$s and scan angle $\alpha_0 = 30°$.

along the $\tilde{t}$ and α_T coordinates, respectively.

Figure 5 presents dependences of the relative SLLs of the distributions $u^{(ph)}_{\text{cnorm}}(0,\alpha_T)$, ($SLL^{(ph)}_{\alpha}$, solid line with squares), $u^{(td)}_{\text{cnorm}}(0,\alpha_T)$ ($SLL^{(td)}_{\alpha}$, dashed line with squares), $u^{(ph)}_{\text{cnorm}}(\tilde{t},\alpha_T=\alpha_0)$ ($SLL^{(ph)}_{\tilde{t}}$, solid line with triangles) and $u^{(td)}_{\text{cnorm}}(\tilde{t},\alpha_T=\alpha_0)$ ($SLL^{(td)}_{\tilde{t}}$, dashed line with triangles) on the chirp sweep range Δf. The pulse length is equal to $\tau_p = 0.1\,\mu$s, and the scan angle is $\alpha_0 = 30°$. The calculated points have been approximated similarly as in Fig. 4. Note that for certain values of Δf (specifically, 400, 600, and 700 MHz), the sidelobes in the $u^{(ph)}_{\text{cnorm}}(0,\alpha_T)$ dependence have not been pronounced. In these cases, the $SLL^{(ph)}_{\alpha}$ estimates have been represented by the $u^{(ph)}_{\text{cnorm}}(0,\alpha_T)$ values calculated for the angles α_T corresponding to the first (highest) sidelobe of the $u^{(td)}_{\text{cnorm}}(0,\alpha_T)$ dependence. These points are encircled in the $SLL^{(ph)}_{\alpha}$ plot.

As already mentioned above when analyzing the plots in Fig. 3, the time-delay scanning is not accompanied by any distortions of the space-time structure of the output signal of the pulse compression filter. As a result, $SLL^{(td)}_{\alpha}$ and $SLL^{(td)}_{\tilde{t}}$ are practically independent of Δf, as can be clearly seen from the plots in Fig. 5. A minor increase observed in the $SLL^{(td)}_{\tilde{t}}$ is explained by the fact that the announced, in the literature, -13.2 dB sidelobe level in compressed chirp pulses [15] is reached only with very large values of the time-bandwidth products $B \to \infty$. At the same time, $SLL^{(ph)}_{\alpha}$ and $SLL^{(ph)}_{\tilde{t}}$ are essentially dependent on Δf. Thus, $SLL^{(ph)}_{\tilde{t}}$ rapidly decreases from approximately -15 dB to nearly -31 dB as Δf changes from 100 to 500 MHz. To all appearance, this is due to increasing the angular sector of effective frequency scanning (this effect was discussed earlier), which results in stronger amplitude modulation of the pulse transmitted toward the target and echo received from it. In this way, an equivalent of a tapered window is realized which leads to sidelobe suppression in the $u^{(ph)}_{\text{cnorm}}(\tilde{t},\alpha_T=\alpha_0)$ dependence. The SLL of the $u^{(ph)}_{\text{cnorm}}(0,\alpha_T)$ dependence first decreases from approximately -26.5 dB to nearly -29 dB as Δf changes from 100 to 500 MHz and then begins to increase monotonically with Δf. Apparently, this effect is explained as follows. The time delay $\Delta^{(ph)}_{\tilde{t}}$ between components m and $m+1$ of the signal $u_{(ph)}(\tilde{t})$ in the case of the phase scanning is determined by the array spacing l and scan angle α_0, *viz.*

$\Delta_{\tilde{t}}^{(ph)} = \frac{l}{c}\sin\alpha_0$. With a fixed pulse length τ_p, the time-bandwidth product B of the signal linearly increases with Δf which results, as follows, from Eq. (19), in decreasing the widths of the main and minor lobes ($\Delta\tilde{t}_{ml}^{(ph)}$ and $\Delta\tilde{t}_{sl}^{(ph)}$, respectively) of the signal $u_{(ph)}(\tilde{t})$. With the AA parameters as specified above and scan angle $\alpha_0 = 30°$, $\Delta_{\tilde{t}}^{(ph)}$ is equal to $0.25\cdot10^{-8}$ s, while $\Delta\tilde{t}_{ml}^{(ph)}$ varies, according to Eq. (19), from $0.225\cdot10^{-7}$ s for $\Delta f = 100$ MHz to approximately $0.29\cdot10^{-8}$ s for $\Delta f = 700$ MHz. As a result, the amount of loss in summation of the m-th components of the signal $u_{(ph)}(\tilde{t})$ increases with Δf. Since the first (highest) sidelobe of component m of the signal $u_{(ph)}(\tilde{t})$ is approximately half as narrow as its main maximum, the first sidelobe in the resultant signal $u_{(ph)}(\tilde{t})$ decreases faster than its main maximum. As a result, the $SLL_{\alpha}^{(ph)}$ magnitude in Fig. 5 decreases with changing Δf from 100 to approximately 450 MHz. At $\Delta f \approx 400$ MHz the characteristic width $\Delta\tilde{t}_{sl}^{(ph)}$ of the sidelobes becomes comparable with the time delay $\Delta_{\tilde{t}}^{(ph)}$. Accordingly, the sidelobes degrade merging with the main peak in a single rather wide maximum. With a further increase of Δf, this maximum diminishes and broadens. As a result, the $SLL_{\alpha}^{(ph)}$ value in Fig. 5 increases quite rapidly as Δf changes from about 450 to 700 MHz.

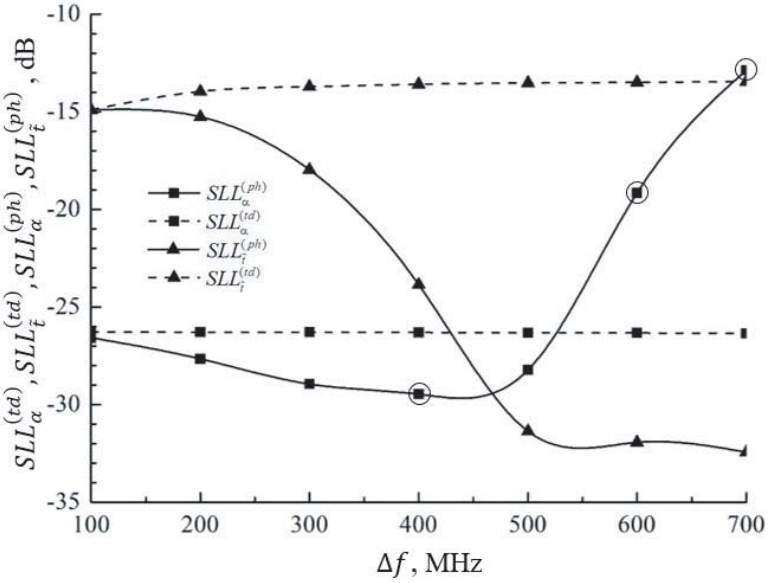

Figure 5. Relative SLLs of the functions $u_{\mathrm{cnorm}}^{(ph)}(0,\alpha_T)$ (solid line with squares), $u_{\mathrm{cnorm}}^{(td)}(0,\alpha_T)$ (dashed line with squares), $u_{\mathrm{cnorm}}^{(ph)}(\tilde{t},\alpha_T=\alpha_0)$ (solid line with triangles) and $u_{\mathrm{cnorm}}^{(td)}(\tilde{t},\alpha_T=\alpha_0)$ (dashed line with triangles) calculated in dependence on the chirp sweep range Δf for the chirp pulse of length $\tau_p = 0.1$ μs and scan angle $\alpha_0 = 30°$.

Thus, the use of the phase scanning in AAs of chirp pulse radars is accompanied by the effects which are similar to those observed in the case of applying tapered windows for reducing the sidelobe levels in the time and space (angular) domains. The magnitude of these effects for a specific AA depends on the frequency sweep range Δf of the sounding signal which should be taken into account when selecting parameters of the tapered function. To increase the admissible frequency sweep range Δf with a given azimuth scanning sector (or the azimuth scanning sector with a given frequency sweep range Δf), a combination of two beamforming techniques can be used (see, for example, [1, 11, 12]). In this case the AA is divided into subarrays, with the phase scanning being used in each of these. The subsection length L_{ss} is to be selected from the condition in Eq. (20) based on the given frequency sweep range Δf and maximum scan angle $\alpha_{0\,\max}$, *viz.*

$$L_{ss} \ll \frac{2c}{\Delta f|\sin\alpha_{0\,\max}|}.$$

The final directional pattern is synthesized through summation of the signals from all subarrays after introducing appropriate time delays between the latter.

5. CONCLUSIONS

The paper presents results of investigating the space-time structure of the output signal of a linear equidistant array of a chirp pulse radar after pulse compression filter, $u_c(\tilde{t}, \alpha_T)$, in dependence on the frequency sweep range Δf of the sounding signal. Distortions of the space-time power pattern $u_{(ph)}(\tilde{t}, \alpha_T)$ observed in such systems in the case of the phase scanning are analyzed. An explanation of these distortions is suggested. It is shown that they are similar to the effects observed in the case of applying taper windows for sidelobe suppression in the time and space (angular) domain. Magnitudes and widths of the main and minor lobes of the space-time power pattern of a phase-scanned array are analyzed as functions of the scan angle with the frequency sweep range being fixed and *vice versa*. Based on the results obtained an applicability condition is suggested for the phase scanning in antenna arrays of chirp pulse radars. It is shown that slight violation of this condition results in decreasing and broadening of the main and minor lobes in the sections of $u_{(ph)}(\tilde{t}, \alpha_T)$ by the planes $\tilde{t} = 0$ and $\alpha_T = \alpha_0$. With strong violations of the phase scanning applicability condition the sidelobes in the $u_{(ph)}(\tilde{t} = 0, \alpha_T)$ dependence degrade merging with the main lobe in a single rather broad maximum. The observed effects can seriously affect the range and azimuth resolution of radars and should be taken into account when selecting parameters of tapered windows. To increase the admissible frequency sweep range with a given azimuth scanning sector (or the azimuth scanning sector with a given frequency sweep range), a combination of two beamforming techniques can be used (see, for example, [1, 11, 12]). In this case, the array antenna is divided into several subarrays, with the phase scanning being used in each of them. The subsection length is to be selected from the phase scanning applicability condition based on the given frequency sweep range and maximum scan angle. The final directional pattern is synthesized through summation of the signals from all subarrays after introducing appropriate time delays between the latter.

REFERENCES

1. Hansen, R. C., *Phased Array Antennas*, John Wiley & Sons, Inc., Hoboken, New Jersey, 2009.
2. Swords, S. S., *Technical History of the Beginnings of Radar*, IEE/Peter Peregrinus, London, 1986.
3. Blanchard, Y., G. Galati, and P. Van Genderen, "The cavity magnetron: Not just a British invention," *IEEE Antennas and Propagation Magazine*, Vol. 55, No. 5, 244–254, 2013.
4. De Size, L. K. and J. F. Ramsay, "Reflecting systems," *Microwave Scanning Antennas, Vol. 1, Apertures*, Ch. 2, 107–213, R. C. Hansen, ed., Academic Press, New York, London, 1964.
5. Cooley, M. E. and D. Davis, "Reflector antennas," *Radar Handbook*, 12.1–12.43, M. I. Skolnik, ed., McGraw-Hill Companies, New York, Chicago, San Francisco et al., 2008.
6. Frank, J. and J. D. Richards, "Phased array radar antennas," *Radar Handbook*, 13.1–13.74, M. I. Skolnik, ed., McGraw-Hill Companies, New York, Chicago, San Francisco et al., 2008.
7. Sturdivant, R. and M. Harris, *Transmit Receive Modules for Radar and Communication Systems*, Artech House, Inc., Boston, London, 2016.
8. Klemm, R., U. Nickel, C. Gierull, P. Lombardo, H. Griffiths, and W. Koch, eds., *Novel Radar Techniques and Applications, Vol. 2, Waveform Diversity and Cognitive Radar, and Target Tracking and Data Fusion*, The Institution of Engineering and Technology, London, 2018.
9. Jeffrey, T. W., *Phased-Array Radar Design: Application of Radar Fundamentals*, SciTech Publishing, Inc., 2009.
10. BCC Research, 2018.5 Key Trends in Radar Technology, *Radar Manufacturing: Global Markets to 2022*, BCC Research Report IAS052A [online], [viewed 15.11.2020], Available from: http://blog.bccresearch.com/5-key-trends-in-radar-technology.
11. Liu, M., L. Zou, and X. Wang, "Practical beamforming technologies for wideband digital array radar," *Progress In Electromagnetics Research Letters*, Vol. 86, 145–151, 2019.

12. Jun, W., C. Duo-Duo, and Y. Fan, "Aperture effect influence and analysis of wideband phased array radar," *Procedia Engineering*, Vol. 29, 1298–1303, 2012.
13. Ajioka, J. S., "Frequency scan antennas," *Antenna Engineering Handbook*, Ch. 19, 19.1–19.30, R. C. Johnson (ed.), Mc-Graw Hill, Inc., New York, Louis, San Francisco, etc., 1993.
14. Mailloux, R. J., *Phased Array Antenna Handbook*, Artech House, Inc., Boston, London, 2005.
15. Cook, C. E. and M. Bernfeld, *Radar Signals: An Introduction to Theory and Application*, Academic Press, New York, London, 1967.
16. Maurice, R. D. A., *Convolution and Fourier Transforms for Communications Engineers*, Pentech Press Ltd., London, 1976.
17. Snieder, R., *A Guided Tour of Mathematical Methods for the Physical Sciences*, Cambridge University Press, Cambridge, 2009.
18. Galushko, V. G., "On application of taper windows for sidelobe suppression in LFM pulse compression," *Progress In Electromagnetics Research C*, Vol. 107, 259–271, 2021.
19. Doerry, A. W., *Catalog of Window Taper Functions for Sidelobe Control*, Technical ReportSAND2017-4042, Sandia National Labs., Albuquerque, New Mexico and Livermore, California, USA, 2017.